Cell, Vol. 96, 363–374, February 5, 1999, Copyright ©1999 by Cell Press

Structural Basis of Rab Effector Specificity: Crystal Structure of the Small G Protein Rab3A Complexed with the Effector Domain of Rabphilin-3A

Christian Ostermeier† and Axel T. Brunger*
The Howard Hughes Medical Institute and
Department of Molecular Biophysics and Biochemistry
Yale University
New Haven, Connecticut 06520

Summary

The small G protein Rab3A plays an important role in the regulation of neurotransmitter release. The crystal structure of activated Rab3A/GTP/Mg^{2+} bound to the effector domain of rabphilin-3A was solved to 2.6 Å resolution. Rabphilin-3A contacts Rab3A in two distinct areas. The first interface involves the Rab3A switch I and switch II regions, which are sensitive to the nucleotide-binding state of Rab3A. The second interface consists of a deep pocket in Rab3A that interacts with a SGAWFF structural element of rabphilin-3A. Sequence and structure analysis, and biochemical data suggest that this pocket, or Rab complementarity-determining region (RabCDR), establishes a specific interaction between each Rab protein and its effectors. RabCDRs could be major determinants of effector specificity during vesicle trafficking and fusion.

Introduction

Rab proteins are a subfamily of the superfamily of regulatory GTP hydrolases (G proteins). The G protein superfamily can be grouped into three categories: (1) small monomeric G proteins, including $p21^{H\text{-}ras}$, Rab3A, Rap1A, and ARF-1; (2) G proteins involved in ribosomal protein synthesis, for example, the elongation factor Tu; and (3) the α subunits (G_α) of heterotrimeric G proteins (for reviews, Bourne et al., 1991; Sigler, 1996; Sprang, 1997a, 1997b). Each member of the G protein family functions as a molecular switch that interacts with its target or effector protein only in the activated, GTP-bound state. The switch is "turned off" by hydrolysis of GTP, causing dissociation of the effector from the G protein. This general mechanism enables G proteins to carry out a wide range of biological tasks, including sorting and amplifying transmembrane signals, directing the synthesis of proteins, regulating vesicular traffic, and controlling cell proliferation and differentiation. All G proteins share a common structural core, but they vary in structural and mechanistic detail. Structures of activated G protein/effector complexes include the ras-binding domain of c-raf1 in complex with Rap1A (Nasser et al., 1995), $p21^{H\text{-}ras}$ in complex with ralGDS (Huang et al., 1998), and G_S-α in complex with the catalytic domains of adenylyl cyclase (Tesmer et al., 1997).

*To whom correspondence should be addressed (e-mail: brunger@laplace.csb.yale.edu).
†Present address: Core Technology Area, Novartis Pharma Research, CH-4002 Basel, Switzerland.

Rab proteins are involved in targeting and regulating vesicular membrane traffic (Ferro-Novick and Novick, 1993; Simons and Zerial, 1993; Fischer von Mollard et al., 1994; Pfeffer, 1994, 1996; Søgaard et al., 1994; Geppert and Südhof, 1998). More than 40 mammalian and 11 yeast Rab proteins have been characterized. All are thought to be isoprenylated at their C terminus (Farnsworth et al., 1991) and are associated with specific subcellular membrane compartments and transport systems (Nuoffer and Balch, 1994; Novick and Zerial, 1997). Rab proteins undergo a functional cycle that is coupled to GTP hydrolysis (Boguski and McCormick, 1993; Nuoffer and Balch, 1994; Pfeffer, 1994; Novick and Zerial, 1997). In the cytosol, Rab proteins are kept in the inactive, GDP-bound state by Rab GDI (GDP-dissociating inhibitor), preventing them from nonspecific binding to membranes. Upon binding to a specific donor compartment or vesicle, GDI is displaced by a GDI displacement factor (GDF). Exchange of GDP to GTP is then catalyzed by GEFs (guanine exchange factors), activating the Rab protein and rendering it resistant to removal from the membrane by Rab GDI (Boguski and McCormick, 1993). Docking or "tethering" of a vesicle to its target membrane may be mediated by specific interactions of the activated, GTP-bound state of the Rab protein with a Rab effector before SNARE (soluble NSF-attachment protein [SNAP] receptor) pairing occurs (Mayer and Wickner, 1997; Ungermann et al., 1998). GTP is hydrolyzed by the intrinsic GTPase activity of the Rab protein. The transition-state barrier of the hydrolysis reaction is lowered by GTPase-activating proteins (GAPs). Once vesicle fusion has occurred, GDI can release the GDP-bound form of Rab to the cytoplasm (Sasaki et al., 1990), and the cycle can begin again.

Rab3A and Rab3C are the most abundant Rab proteins in neurons and are predominantly localized to synaptic vesicles (Fischer von Mollard et al., 1990). Gene knockout of these Rab proteins impairs regulation of neurotransmitter release (Castillo et al., 1997; Geppert et al., 1997). The GTP-bound form of Rab3A interacts with at least two effector proteins, rabphilin-3A (Stahl et al., 1996) and rim (Wang et al., 1997), which may interact with, as of yet unknown, downstream targets. Comparative studies of wild-type and Rab3A knockout mice have demonstrated interactions between Rab3A and rabphilin-3A in vivo; rabphilin-3A levels are decreased by 70% in Rab3A knockout mice despite normal mRNA levels, suggesting degradation of uncomplexed rabphilin-3A protein in vivo (Li et al., 1994). Furthermore, Rab3A may be required for transporting rabphilin-3A from the neuronal cell body to the synapse, since rabphilin-3A is retained in the cell body of Rab3A-defective neurons (Li et al., 1994). Activated Rab3A reversibly recruits rabphilin-3A to synaptic vesicles (Stahl et al., 1996). Rim has sequence similarity to rabphilin-3A but localizes to the active zone of the presynaptic plasma membrane instead of to synaptic vesicles (Wang et al., 1997). Rab3A–effector interactions are also important for cortical granule exocytosis (Conner and Wessel, 1998).

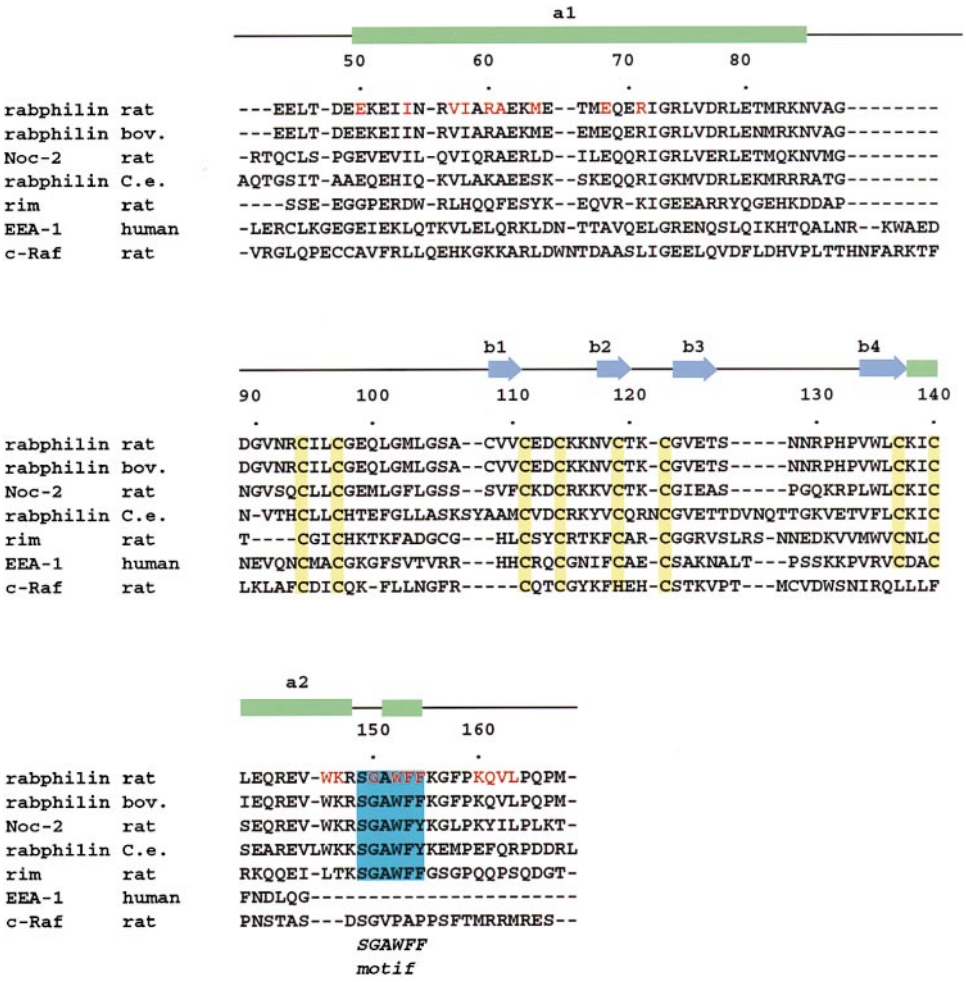

Figure 1. Sequence Alignment of Proteins Similar to the Effector Domain of Rabphilin-3A

Numbering and secondary structural elements (green, α helix; blue arrow, β strand) are shown for rabphilin-3A. The conserved cysteine residues that are responsible for Zn^{2+} binding are shaded in yellow. The SGAWFF structural element is shaded in blue. A residue marked in red indicates a contact between the particular residue and Rab3A in the crystal structure of the Rab3A/rabphilin-3A complex.

Rabphilin-3A consists of the N-terminal Rab3A effector domain, a proline-rich linker region, and two tandem C2 domains (Yamaguchi et al., 1993). The sequences of the C2 domains are similar to those of synaptotagmin and protein kinase C (Yamaguchi et al., 1993), and they probably have the same tertiary structure (Sutton et al., 1995). Similar to other C2 domains, the C2 domains of rabphilin-3A bind to phosphatidylinositol 4,5-bisphosphate-containing vesicles in a Ca^{2+}-dependent manner (Chung et al., 1998). The proline-rich linker region is targeted by cAMP-dependent protein kinase and Ca^{2+}/calmodulin-dependent protein kinase II (Kato et al., 1994; Fyske et al., 1995). The rabphilin-3A effector domain binds specifically to the activated GTP-bound state of Rab3A (Shirataki et al., 1993; Li et al., 1994) and possesses two conserved Zn^{2+}-binding $CX_2CX_{13,14}CX_2C$ sequence motifs whose cysteines are sensitive to mutation (Stahl et al., 1996). Similar motifs are also found in other Rab effectors, including rim (Wang et al., 1997) and EEA1 (Gaullier et al., 1998; Patki et al., 1998; Simonsen et al., 1998; Wiedemann and Cockcroft, 1998) (Figure 1).

Here, we present the crystal structure of activated Rab3A in complex with the effector domain of rabphilin-3A at 2.6 Å resolution. The structure was solved using multiwavelength anomalous dispersion (MAD) phasing (Hendrickson, 1991) with selenomethionine (SeMet) labeled complex. The Rab3A/rabphilin-3A interface involves the conserved switch I and II regions and a distinct pocket on the surface of Rab3A (referred to as RabCDR) whose sequence varies among members of the Rab family. We propose that all Rab proteins use RabCDRs to mediate specific interactions with downstream effectors.

Results and Discussion

Characterization and Purification of a Rab3A/Rabphilin-3A Complex

Residues 45–161 of the rabphilin-3A effector domain are sufficient for binding to Rab3A (data not shown). For our structural studies, a somewhat larger fragment, residues

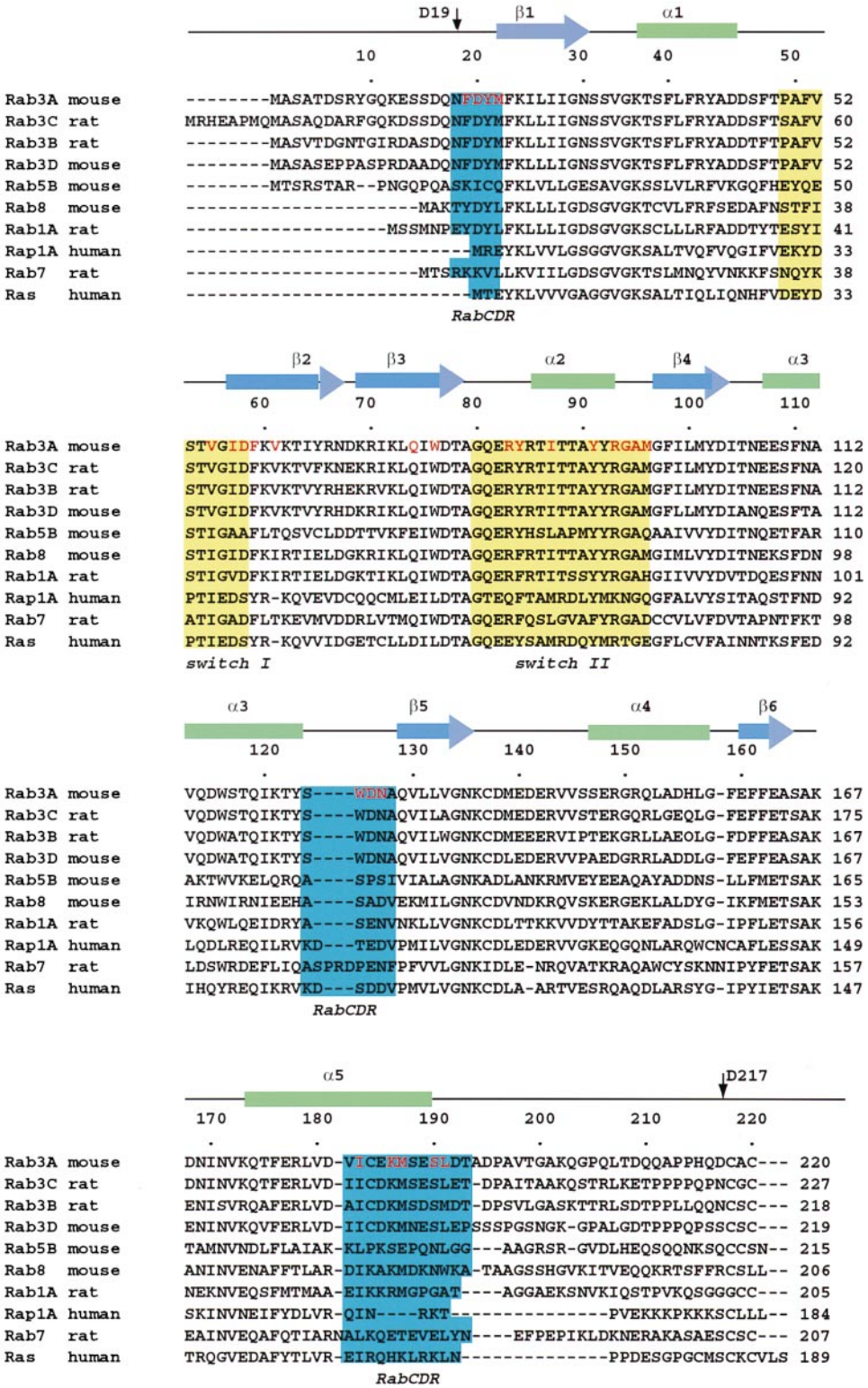

Figure 2. Sequence Alignment of Rab Proteins

Numbering and secondary structural elements (green, α helix; blue arrow, β strand) are shown for Rab3A. Switch I and II regions and the RabCDR are shaded in yellow and blue, respectively. A residue marked in red indicates a contact between the particular residue and rabphilin-3A in the crystal structure of the Rab3A/rabphilin-3A complex.

Table 1. Crystallographic Data, Phasing, and Refinement

Space group	C2					
Cell dimensions	a = 89.32 Å, b = 95.62 Å, c = 47.72 Å, β = 94.49°					
	d_{min} (Å)	No. of Measurements	No. of Unique Reflections	Completeness (%)	I/σ	R_{sym}[a,b] (%)
SeMet λ_1 (0.9879 Å)	2.6	58,641	23,889	98.5 (97.8)	17.9	4.9 (31.7)
SeMet λ_2 (0.9793 Å)	2.6	58,755	23,968	98.6 (97.8)	16.8	5.2 (39.8)
SeMet λ_3 (0.9789 Å)	2.6	58,860	23,992	98.7 (97.9)	15.8	5.1 (39.6)

Observed diffraction ratios[c]

	λ_1	λ_2	λ_3
λ_1	0.124	0.084	0.091
λ_2		0.141	0.078
λ_3			0.146

Phasing power[d] and figure of merit (FOM)

	$\lambda_1 \rightarrow \lambda_1^-$	$\lambda_1 \rightarrow \lambda_2^+$	$\lambda_1 \rightarrow \lambda_2^-$	$\lambda_1 \rightarrow \lambda_3^+$	$\lambda_1 \rightarrow \lambda_3^+$	FOM
40–2.6 Å	0.75	1.33	1.45	1.07	1.30	0.52
2.7–2.6 Å	0.27	0.42	0.50	0.38	0.47	0.24

Refinement

Resolution range	500–2.6 Å										
No. of reflections	23,478										
Resolution (Å)	500–5.6	4.45	3.88	3.53	3.28	3.08	2.93	2.80	2.69	2.6	Overall
R value[e]	24.4	18.4	19.1	22.1	23.7	27.0	28.4	30.9	30.0	29.6	23.3
R_{free}[f]	24.0	21.7	23.5	25.3	26.7	33.4	29.8	31.5	39.1	31.1	26.4
Luzzati coordinate error	0.36 Å										
Cross-validated Luzzati coord. error	0.43 Å										
Bond-length deviation	0.006 Å										
Bond-angle deviation	1.10°										
Improper-angle deviation	0.63°										
Dihedrals	21.3°										
Average B factor	50.5 Å^2										
Rmsd for bonded main chain atoms	2.7 Å^2										
Rmsd for bonded side chain atoms	4.1 Å^2										
Minimum B factor	8.8 Å^2										
Maximum B factor	124 Å^2										
Residues in core φ-ψ region (%)	86.1%										
Residues in disallowed regions (%)	0.0%										

[a] Values in parentheses are for the high-resolution bin.

[b] $R_{sym} = \Sigma_h\Sigma_i|I_i(h) - \langle I(h)\rangle|/\Sigma_h\Sigma_i I_i(h)$, where $I_i(h)$ is the i-th measurement and $\langle I(h)\rangle$ is the mean of all measurements of I(h) for Miller indices h.

[c] Values are $\langle(\Delta|F|)^2\rangle^{1/2}/\langle|F|^2\rangle^{1/2}$, where Δ|F| is the dispersive (off-diagonal elements), or Bijvoet difference (diagonal elements), computed between 20 and 2.6 Å resolution.

[d] MAD phasing power is defined as $[\langle|F_D - F_N|^2\rangle/\int_\Phi P(\Phi)(||F_N|e^{i\Phi} + \Delta F_h| - |F_D|)^2 d\Phi]^{1/2}$, where P(Φ) is the experimental phase probability distribution. F_N corresponds to the structure factors at the reference wavelength λ_1, F_D corresponds to the structure factors at wavelength λ_i (indicated by a superscript "+") or its Friedel mate (indicated by a superscript "−"), and F_h is the difference in heavy atom structure factors between the two wavelengths.

[e] $R = \Sigma(|F_{obs}| - k|F_{calc}|)/\Sigma|F_{obs}|$.

[f] Free R value is the R value obtained for a test set of reflections, consisting of a randomly selected 10% subset of the diffraction data, not used during refinement.

40–170, was chosen to maximize the inclusion of structural elements based on secondary structure prediction (Garnier, et al., 1996). After recombinant expression, attempts to purify these fragments failed due to aggregation and proteolysis. Dual-plasmid coexpression yielded stable complex of rabphilin-3A and the catalytically inactive Q81L mutant of Rab3A. This complex was not prone to aggregation or degradation of rabphilin-3A. Complex formation with Rab3A may have induced proper folding of rabphilin-3A during bacterial expression.

The rabphilin family contains several cysteine residues, which may interfere with structural studies (Figure 1). Eight out of the nine cysteines of rabphilin-3A [40–170] are highly conserved and are involved in Zn^{2+} binding. Cys-108, which is not conserved, was changed to serine by site-directed mutagenesis. This residue is not involved in Zn^{2+} binding and did not affect complex formation (data not shown).

The C-terminal residues of a specific Rab protein localize it to a specific membrane in the cell (Chavrier et al., 1991). This targeting specificity may be correlated with sequence variability in the C-terminal region, residues 195–220 of Rab3A (Figure 2). In the neuron, the C-terminal residues Cys-218 and Cys-220 of Rab3A are posttranslationally modified by geranyl-geranylation (Farnsworth et al., 1991). In order to prevent oxidation of the unmodified cysteines in bacterially expressed protein, these residues were deleted from Rab3A by truncation. To improve chances of crystallization, additional C-terminal truncations were carried out since this region is unstructured in the Rab7 homolog (Neu et al., 1997). Using secondary structure prediction to maximize

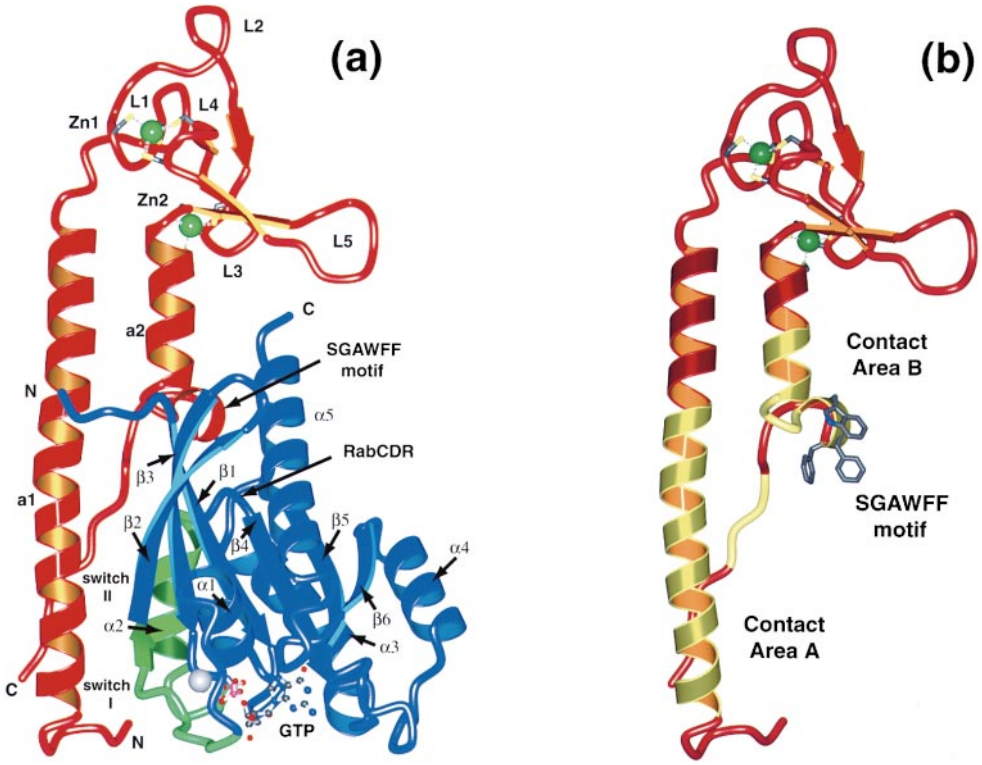

Figure 3. Rab3A/Rabphilin-3A Complex

(a) Ribbon diagram of the Rab3A/GTP/Mg^{2+}/rabphilin-3A complex. Rab3A is shown in blue, rabphilin-3A in red, the GTP is shown as balls and sticks, and Mg^{2+} and Zn^{2+} are shown as gray and green balls, respectively. The putative switch I and II regions of Rab3A are labeled in green. Secondary structural elements of Rab3A are labeled with Greek characters followed by a numeral. Prepared using BOBSCRIPT (Esnouf, 1997), gl-render, MOLSCRIPT (Kraulis, 1996), and POV-ray (The POV-ray team, 1998).

(b) Ribbon diagram of contact areas of rabphilin-3A that interact with Rab3A (yellow). The SGAWFF structural element (balls and sticks) is localized C terminal of α helix α2 of rabphilin-3A.

the extent of secondary structural elements, several truncation mutants of Rab3A were expressed: [1–217], [19–217], [22–217], [1–198], [19–198], [22–198], [1–188], [19–188], and [22–188]. Deletion of the N-terminal residues 1–18 of Rab3A did not prevent binding to rabphilin-3A [40–170], whereas deletion of residues 1–21 of Rab3A entirely abolished binding. The selected C-terminal truncations of Rab3A did not affect binding to rabphilin-3A [40–170]. The resulting complexes of truncated Rab3A and rabphilin-3A [40–170] were stable and monomeric with 1:1 stoichiometry as determined by SDS-PAGE, native PAGE, gel filtration, and multiangle laser light scattering (data not shown).

Crystallization and Structure Determination

Crystals of several of the truncated complexes were obtained by sparse matrix screening: rabphilin-3A C108S [40–170]/Rab3A Q81L [1–217], rabphilin-3A C108S [40–170]/Rab3A Q81L [19–217], rabphilin-3A C108S [40–170]/Rab3A Q81L [19–198], rabphilin-3A C108S [40–170]/Rab3A Q81L [19–188], all of which included GTP/Mg^{2+}. The crystals of all the complexes belonged to space group C2 with similar unit cell parameters, a = 89 Å, b = 94 Å, c = 47 Å, and β = 94° and 55% solvent content. The Rab3A Q81L [19–217]/GTP/Mg^{2+}/rabphilin-3A C108S [40–170] complex (in the following referred to as Rab3A/rabphilin-3A complex) produced diffraction to the highest resolution and was therefore used for structure determination. The choice of cryoprotectant was critical to avoid high crystal mosaicity. The best diffraction quality was obtained by using 12.5% erythritol in a low-salt buffer, although individual crystals exhibited a high degree of variability in diffraction quality. The Rab3A/rabphilin-3A complex structure was solved using MAD phasing with SeMet labeled protein complex (Table 1). Zinc has a considerable anomalous signal at the wavelengths used for SeMet MAD phasing, requiring inclusion of the Zn^{2+} sites in the MAD phasing calculations. The f′ and f′′ components of the selenium and zinc atomic scattering factors were independently refined during MAD phasing. The experimental MAD phases were used throughout the refinement and model building process in order to reduce model bias (Pannu et al., 1998). The final free R value is 26.4% for all reflections in the test set with Bragg spacing between 500 and 2.6 Å.

Structure of Rab3A Q81L

The structural core of Rab3A is a guanine nucleotide–binding domain consisting of a central six-stranded β sheet flanked by α helices (Figure 3a and Dumas et al., 1998). It is similar to the catalytic core of other G proteins, such as $p21^{H\text{-}ras}$ (Tong et al., 1989; Brunger et al., 1990; Pai et al., 1990). We defined the switch I and switch II regions of Rab3A by analogy to the observed structural differences in the GTP- and GDP-bound forms of $p21^{H\text{-}ras}$ (Figure 7 in Milburn et al., 1990). In the Rab3A/

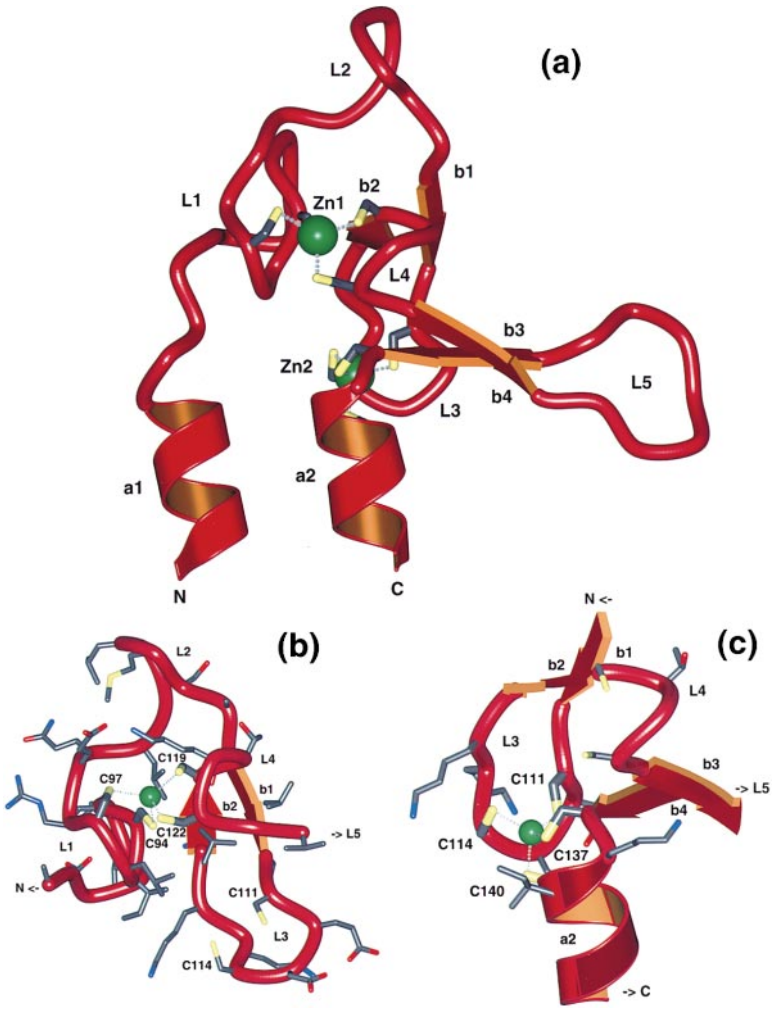

Figure 4. Zinc-Binding Domain of Rabphilin-3A

(a) Ribbon diagram of the zinc-binding domain of rabphilin-3A. The domain consists of five loops that are interconnected by two zinc ions, Zn1 and Zn2 (shown in green). The five loops and the four short β strands are as follows: loop L1 (residues 88–97), loop L2 (residues 100–107), b1 (residues 108–110), loop L3 (residue 108–116), b2 (residues 117–119), loop L4 (residues 118–122), b3 (residues 123–126), loop L5 (residues 126–134), and b4 (residues 134–137).

(b) Close-up view of the Zn1-binding site.

(c) Close-up view of the Zn2-binding site.

rabphilin-3A complex, these switch regions interact with rabphilin-3A (Figure 3a). However, a precise definition of the switch regions of Rab3A must await structure determination of the inactive GDP-bound form of Rab3A.

By analogy to other G proteins, the conserved Gln-81 residue stabilizes the catalytic transition state. The Q81L mutation lowers the catalytic rate of Rab3A and locks it into the activated, GTP-bound state (Der et al., 1986; Prive et al., 1992). The GTP-bound state of the Q81L mutant of Rab3A was confirmed by connected electron density for the three nucleotide phosphate groups, using $|F_{obs}|e^{i\varphi}$ electron density maps calculated from experimental MAD phases (data not shown).

Rabphilin Zn^{2+}-Binding Domain

Two striking features of the rabphilin-3A [40–170] structure are a 34-residue α helix and a domain containing two zinc ions (Figure 3b). The Zn^{2+}-binding domain of rabphilin-3A consists of five loops, numbered L1 through L5 (Figure 4a). The termini of loops L3 and L5 are flanked by four short β strands, termed b1–b4. A zinc ion, Zn1, is coordinated by Cys-94 and Cys-97 of loop L1, and Cys-119 and Cys-122 of loop L4 (Figure 4b). Another zinc ion, Zn2, is coordinated by Cys-111 and Cys-114 of loop L3, and Cys-137 and Cys-140 of α helix a2 (Figure 4c). The coordinating cysteine pairs comprising the two Zn^{2+}-binding sites are thus interspersed in sequence space. In both cases, the coordination geometry is nearly tetrahedral. A structural core is formed by the two Zn^{2+}-binding sites and by an adjacent hydrophobic cluster consisting of isoleucine, leucine, and valine residues (Figures 4b and 4c). Extended loops (L2 and L5) and α helices (a1 and a2) protrude from this core. Since this core does not directly interact with Rab3A, a possible role of the Zn^{2+}-binding domain is to provide a structural support for the rest of the rabphilin-3A effector domain. Indeed, mutagenesis of the Zn^{2+}-coordinating cysteines abolished binding to Rab3A, presumably caused by misfolding of the Zn^{2+}-binding domain (Stahl et al., 1996).

A DALI search (Holm and Sander, 1993) revealed only limited structural similarity between the rabphilin-3A Zn^{2+}-binding domain and other zinc-binding domains with the closest match (overall root-mean-square difference 3.5 Å) being the LIM domain of cysteine-rich intestinal protein (Pérez-Alvarado et al., 1996). LIM domains have the consensus sequence $CX_2CX_{16-23}HX_2CX_2CX_2CX_{16-23}CX_{2-3}$(C,H,D), which is different from that of rabphilin-3A. LIM domains are found in several proteins that are involved in cell growth and differentiation,

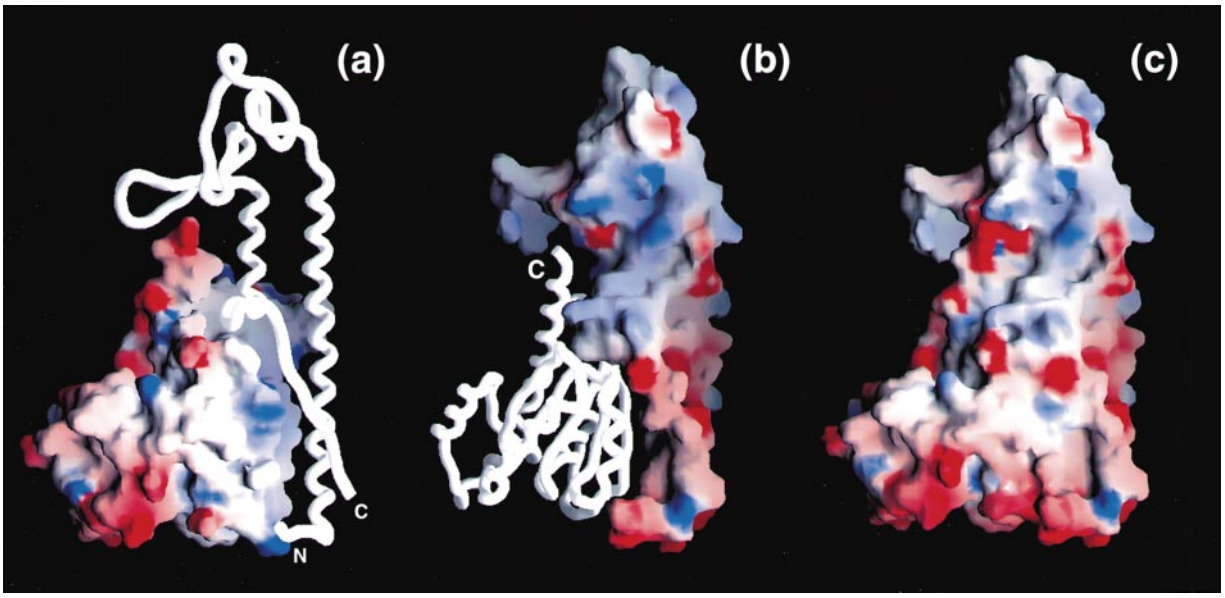

Figure 5. Surface Charge Distribution

Calculated surface electrostatic potential (a) of Rab3A (rabphilin-3A is shown as a ribbon diagram), (b) of the effector domain of rabphilin-3A (Rab3A is shown as a ribbon), and (c) of the Rab3A/rabphilin-3A complex. The color scale for the charge distribution extends from -10 kT/e$^-$ to $+10$ kT/e$^-$; blue, positive; red, negative charge. Calculations were carried out with GRASP (Nicholls et al., 1991).

and they mediate specific protein–protein interactions (Schmeichel and Beckerle, 1994, 1998; Gill, 1995; Johnson et al., 1997). LIM domains and the rabphilin-3A Zn^{2+} domain have in common that they both serve as structural support for other structural elements.

Interactions of Rab3A with Rabphilin-3A

The Rab3A/rabphilin-3A complex buries a surface area of 2800 Å^2, most of which involves hydrophobic interactions (Figures 5a and 5b). The few ionic and polar interactions between Rab3A and rabphilin-3A are characterized by a largely complementary charge distribution on their respective molecular surfaces (Figures 5a and 5b).

There are two distinct interfaces (Figure 3b) with buried surface areas of 1300 Å^2 and 1500 Å^2, respectively. The first one, contact area A, consists of parts of the switch I and switch II regions of Rab3A, the rabphilin-3A α helix a1, and the C-terminal extended polypeptide segment of rabphilin-3A (Figure 6c). The interactions with the rabphilin-3A C-terminal segment may explain the lack of binding of rabphilin-3A truncation mutants that terminate at residue 157 (McKiernan et al., 1996). The second interface, contact area B, involves the C-terminal end of the rabphilin-3A α helix a2 and the adjacent SGAWFF structural element (Figures 6a and 6b). The SGAWFF structural element interacts with the RabCDR consisting of residues 19–22, loops α2-β4 and α3-β5, and the C-terminal half of α helix α5 (Figure 6a). Residues 19–22 of the RabCDR are essential for Rab3A/rabphilin-3A complex formation; deletion of these residues abolishes binding to rabphilin-3A. A conspicuous feature of the SGAWFF structural element is the perpendicular edge-to-plane configuration of a tryptophan and two phenylalanine residues, typical for aromatic ring interactions (Figures 6a and 6b) (Burley and Petsko, 1985).

Structural changes in Rab3A occur upon complex formation with rabphilin-3A in two loops, α2-β4 and α3-β5 (Figure 6a). These loops are presumably flexible in uncomplexed Rab3A as judged by the weak electron density in the crystal structure of uncomplexed Rab3A (Dumas et al., 1998) but become significantly more ordered in the Rab3A/rabphilin-3A complex (Figure 6b).

The structure of the Rab3A/rabphilin-3A complex is different from that of other known G protein/effector complexes, including Rap1A/c-raf1 (Nasser et al., 1995), Ras/RalGDS (RID) (Huang et al., 1998), and G_s-α in complex with the catalytic domains of adenylyl cyclase (Tesmer et al., 1997). In the case of Rap1A/c-raf1, complex formation is mediated by an antiparallel β–β interaction between a strand of the Rap1A switch I region and a strand of the Ras-binding domain of c-raf1 (Marshall 1993; Polakis and McCormick, 1993; Nasser et al., 1995). It is unknown whether the c-raf1 Zn^{2+}-binding domain interacts with Rap1A or Ras (Brtva et al., 1995), since the crystal structure did not include this domain. Furthermore, the isolated raf Zn^{2+}-binding domain structure (Mott et al., 1996) is very different from that of rabphilin-3A. The interactions between Ras and RalGDS (RID) (Huang et al., 1998) are similar to that of Rap1A/c-raf1 with the exception of a second effector molecule that is bound to the switch II region of Ras.

Specificity of Rab/Effector Interactions

The SGAWFF motif is conserved among members of the rabphilin family, including rim and Noc2, while it is absent in other G protein effectors, such as c-raf1 or EEA1 (Figure 1). Similar to rabphilin-3A, rim has two

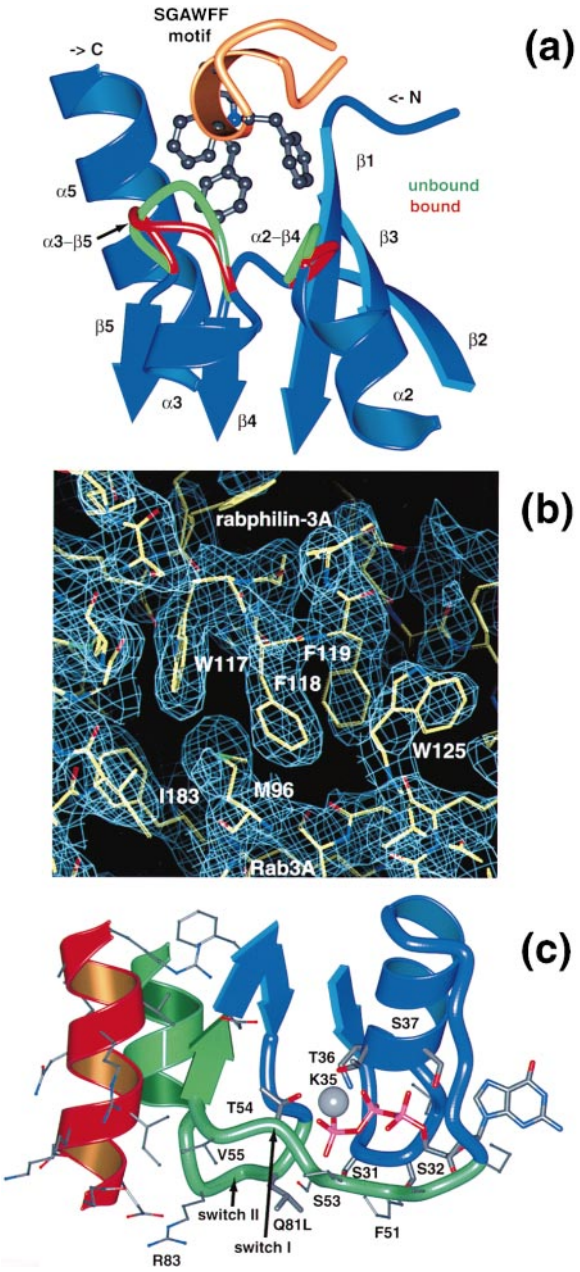

Figure 6. Interfaces between Rab3A and Rabphilin-3A

(a) Comparison of rabphilin-3A-bound (red ribbon diagram) and uncomplexed (green ribbon diagram) Rab3A (Dumas et al., 1998). Upon complex formation, loops α2-β4 and α3-β5 are pushed apart by "induced fit."

(b) Interactions between the RabCDR of Rab3A and the SGAWFF structural element of rabphilin-3A. The refined model (sticks) is superimposed on the experimental electron density map (blue) obtained by MAD phasing and subsequent density modification, contoured at 1.0 σ.

(c) Ribbon diagram of the interactions of rabphilin-3A (red) with the switch I and II regions (green) of Rab3A. Selected residues are shown as balls and sticks. Mg^{2+} is shown as a gray sphere.

$CX_2CX_nCX_2C$ Zn^{2+}-binding motifs, although the overall sequence identity is low, and loop L5 is significantly longer. Rim is predicted to contain an α helix that may interact with the switch regions of Rab3A in a similar manner as rabphilin-3A. Rim binds with high specificity to both Rab3A and Rab3C (Wang et al., 1997). Both Rab3A and Rab3C have nearly identical RabCDRs (Figure 2), and they both form complexes with rabphilin-3A or rim. However, the sequence of the RabCDR of other Rab proteins is very different from that of Rab3A (Figure 2), and these other Rab proteins do not bind to rabphilin-3A (Li et al., 1994). These observations can be explained if binding specificity of Rab3A and Rab3C is primarily determined by contact area B, the interface between the SGAWFF structural element of the effector and the RabCDR of the Rab protein (Figures 1 and 2). The sequence variability of the RabCDR in the Rab family (Figure 2) thus could be correlated with binding specificity for Rab/effector pairing. Binding specificity may be due to the complementary shape of the rabphilin-3A and Rab3A surfaces (Figures 6a and 6b).

RabCDRs may represent a general principle of G protein–effector interactions. For example, the α3-β5 loop of the yeast Rab protein Ypt1p is probably involved in Ypt1p localization to the Golgi (Brennwald and Novick, 1993). Likewise, the α3-β5 loop and the N terminus of the β1 strand of Rab5 probably interact with effectors that confer specific membrane association (Stenmark et al., 1994). The α3-β5 loop of the heterotrimeric G protein $G_{S\alpha}$/GTPγS interacts with the catalytic domain of adenylyl cyclase (Sunahara et al., 1997; Tesmer et al., 1997). In addition to this structural evidence, biochemical data further support the importance of the α3-β5 loop. It is important for interactions between $G_{t\alpha}$ and the cGMP phosphodiesterase γ subunit (Rarick et al., 1992), and for interactions between $G_{S\alpha}$ and adenylyl cyclase (Berlot and Bourne, 1992).

Model for a Rab Switch

Since no structure of the GDP-bound form of Rab3A is available, one can only speculate about induced structural changes upon GTP hydrolysis. Assuming that similar structural changes upon GTP hydrolysis occur in both $p21^{H\text{-}ras}$ (Milburn et al., 1990) and Rab3A, GTP hydrolysis would be accompanied by extensive structural changes in the switch regions of Rab3A. Thr-54 would link GTP hydrolysis to structural changes in the switch regions through its interaction with the γ-phosphate of the bound nucleotide (Figure 6c). GTP hydrolysis would result in an outward movement of switch I, a coil–helix transition at the N terminus of switch II, and subsequent reorientation of the α2 helix (Figure 7 in Milburn et al., 1990). Both regions are involved in extensive interactions with rabphilin-3A. These putative conformational transitions would destabilize the Rab3A/rabphilin-3A complex, eventually leading to dissociation (Figure 7). One cannot rule out that structural changes also occur in the rabCDR, since the β2-β3 hairpin is also affected by GTP hydrolysis in ARF-1 (Figure 2 in Goldberg, 1998). However, ARF-1 might represent a special case since this hairpin is unaffected by GTP hydrolysis in known structures of other small G proteins and heterotrimeric G proteins.

Rabphilin Function

The electrostatic potential surface of the Rab3A/rabphilin-3A complex has a highly asymmetric distribution

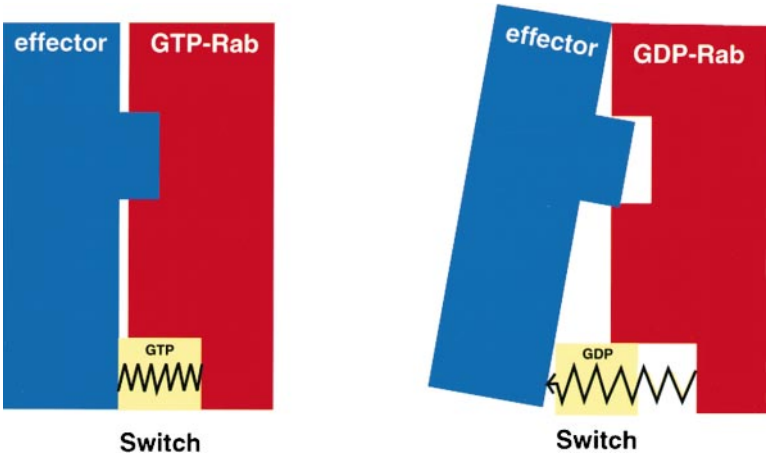

Figure 7. Rab Switch Model

Binding specificity is determined by the shape complementarity of the second binding site. GTP hydrolysis leads to a conformational transition in the switch I and II regions, resulting in dissociation of the Rab3A/rabphilin-3A complex.

(Figure 5c). Furthermore, the C-terminal geranyl-geranylated cysteines of Rab3A interact with the vesicular membrane. These observations suggest a particular orientation of the Rab3A/rabphilin-3A relative to the membrane surface (top in Figure 5c). The positively charged Zn^{2+}-binding domain of complexed rabphilin-3A would thus be close to the negatively charged membrane surface. The localization of rabphilin-3A to synaptic vesicles by Rab3A (Stahl et al., 1996) may therefore promote interactions between the rabphilin-3A Zn^{2+}-binding domain and its associated loops with vesicular membrane components or the cytoskeleton.

The rabphilin-like EEA1 protein colocalizes with Rab5, and the C-terminal domain of EEA1 contains a Zn^{2+}-binding domain that binds phosphatidylinositol-3-phosphate (PtdIns(3)P) with high specificity (Gaullier et al., 1998; Patki et al., 1998; Simonsen et al., 1998; Wiedemann and Cockcroft, 1998). Mutants of EEA1 defective in Zn^{2+}-binding lost their ability to bind to PtdIns(3)P. The sequences of the EEA1 and rabphilin Zn^{2+}-binding domains are related (Figure 1), suggesting that the rabphilin Zn^{2+}-binding domain may also bind to phospholipids.

Noc2 is a soluble, cytoplasmic protein of 38 kDa molecular weight with high sequence similarity to the effector domain of rabphilin-3A (Figure 1). In contrast to rabphilin-3A, it lacks the two C2 domains. Noc2 is expressed predominantly in endocrine tissue and hormone-secreting cell lines and at very low levels in brain (Kotake et al., 1997). Noc2 interacts with the LIM domain–containing protein zyxin, a component of the cytoskeleton. Noc2 may therefore be involved in regulating exocytosis by interaction with the cytoskeleton (Kotake et al., 1997).

The effector domain of rabphilin-3A binds to α-actinin, a factor that cross-links actin filaments during Ca^{2+}-dependent exocytosis (Kato et al., 1996). Binding of rabphilin-3A to Rab3A/GTPγS inhibits the interaction with α-actinin (Kato et al., 1996). Therefore, the rabphilin-3A/Rab3A complex may play a central role in regulation of actin filament reorganization before synaptic vesicle fusion occurs. One could speculate that activated Rab3A prevents actin filament reorganization by sequestering all free rabphilin-3A molecules. Upon GTP hydrolysis, rabphilin-3A would be released and would be available to reorganize actin filaments. Rab3A may thus act as a timer to prepare synaptic vesicles for docking or fusion by filament reorganization.

Conclusions

Rab proteins have several distinct functions in secretory and endocytic pathways (Novick and Zerial, 1997), and they are part of an extensive network of effectors, GTPase activating proteins, and exchange factors (GDIs, GEFs, and GAPs). Multiple Rab systems exist in the same cell, requiring highly specific interactions between particular Rabs and their effectors, such as the Rab3A/rabphilin-3A complex in presynaptic terminals. Considering the relative sequence conservation of the switch I and II regions (Figure 2), the corresponding protein–protein interface is probably insufficient for specific Rab protein/effector binding. In contrast, the effector interactions involving the hypervariable RabCDR are likely to provide more target specificity. The RabCDR is an example of a more general G protein/effector interface, such as that found in the complex of $G_{S\alpha}$ with adenylyl-cyclase (Sunahara et al., 1997; Tesmer et al., 1997). We propose that RabCDRs are regions of variable sequence among the Rab family (Figure 2) within a structurally conserved framework. The combination of the variable RabCDR and the conserved switch mechanism enables Rab proteins to interact with a wide variety of effectors in both a highly specific and activation state–dependent manner. RabCDRs are probably key determinants for the regulation of vesicle traffic and fusion.

Experimental Procedures

Cloning and Expression

Using pET15 expression vectors (Novagen) containing Rab3A 1–217 and Rab3A Q81L [1–220] (kindly provided by P. DeCamilli), the Rab3A Q81L [1–217] fragment was obtained by standard cloning techniques and was cloned into the pET15b vector. The resulting construct had a thrombin cleavable N-terminal hexahistidine tag. The Rab3A Q81L [19–217] truncation mutant was subcloned using the following PCR primers: TCA GAC CAT ATG TTC GAC TAT ATG TTC and GCA GCC GGA TCC TC. The rabphilin-3A [40–170] fragment was subcloned into pET28a (Novagen) by using a pGEX-KG plasmid (Guan and Dixon, 1991) carrying rabphilin-3A, residues 1–170, as template (Stahl et al., 1996, kindly provided by R. Jahn). The following primers were used for PCR: CAG ACG GAC CAT ATG AGG AAG CAG GAA G and GCT TGAGCT CGA GTC GAC CTA C.

Cysteine-108 of the rabphilin-3A [40–170] fragment was changed to serine by site-directed mutagenesis (QuikChange, Stratagene). All DNA sequences were verified by dideoxynucleotide sequencing (HHMI Biopolymer and W. M. Keck Biotechnology Resource Laboratory, Yale University). Both plasmids, Rab3A Q81L [19–217] in pET15b and rabphilin C108S [40–170] in pET28a, were subsequently transformed into BL21(DE3) cells (Novagen) and cultured in presence of ampicillin and kanamycin. Cells were grown in terrific broth (TB) medium containing 50 mg/l kanamycin and 100 mg/l ampicillin and induced with 0.8 mM isopropyl-1-thiogalactopyranoside (IPTG) at 25°C at an optical density of $A_{600nm} = 1$. After 3 hr, the cells were harvested by centrifugation and stored at −80°C. Cells were homogenized in 100 mM Tris (pH 7.9), 200 mM NaCl, 5 mM $MgCl_2$, 10% glycerol, and 0.5% Triton X-100 using sonication. The lysate was centrifugated for 30 min at 35,000 g. The supernatant was incubated with Ni-NTA resin (Quiagen) for 1 hr at 4°C. The resin was packed into a column and washed with 50 mM Tris (pH 7.9), 100 mM NaCl, 5 mM $MgCl_2$, and 5 mM imidazole. The His-tagged proteins eluted at 200 mM imidazole. Thrombin (Haematologic Technologies Inc.) was added at a concentration of 0.5 mg/l, and the mixture was dialyzed at 4°C for 10 hr against 20 mM Tris (pH 8.5), 2.5 mM $MgCl_2$. After dialyzing, the protein was loaded onto a MonoQ column (Pharmacia) and eluted with a linear gradient from 0 mM to 200 mM NaCl. Fractions containing the complex were pooled, concentrated, and loaded onto a Superdex-200 (Pharmacia) size exclusion column equilibrated with 10 mM Tris (pH 8.0), 2.5 mM $MgCl_2$. The protein was concentrated to 10–20 mg/ml. Protein concentrations were determined using the Bradford protein concentration assay (Biorad) that was calibrated with bovine serum albumin standard. SeMet protein was produced essentially as above, except for the following: B834Iλ(DE3) cells (Novagen) were used for expression and were grown in SeMet-containing defined media (Leahy et al., 1994). Purification, crystallization, and cryoprotection were done under reducing conditions: 5 mM β-mercaptoethanol during metal chelate chromatography, 2 mM 2,4-dithiothreitol (DTT) during all other purification steps, and 20 mM DTT during crystallization.

Crystallization, Data Collection, and Processing

Crystals grew by hanging drop vapor diffusion at 20°C. Two microliters of 10–20 mg/ml protein were mixed with 2 μl of mother liquor, consisting of 100 mM Tris (pH 8.0), 200 mM $MgSO_4$, 20% PEG 4000 (Hampton Research), on a siliconized glass coverslip and equilibrated against 1 ml of mother liquor. Rod-shaped crystals grew to full size (0.6 mm × 0.3 mm × 0.2 mm) after 48 hr. Crystals were cryoprotected in 100 mM Tris, 20% PEG 4000, and 12.5% erythritol, and then flash-frozen in liquid nitrogen–cooled propane. SeMet crystals were grown and cryoprotected in the presence of 20 mM DTT.

The Rab3A Q81L [19–217]/GTP/Mg^{2+}/rabphilin-3A C108S [40–170] complex crystallized in space group C2 with one complex per asymmetric unit. MAD data were collected using three wavelengths (Table 1) at 100 K at beamline X4A of the National Synchrotron Light Source (NSLS). Data were processed using DENZO (Otwinowski and Minor, 1998), and intensities were reduced and scaled using SCALEPACK (Otwinowski and Minor, 1998) (Table 1).

Structure Determination, Refinement, and Model Quality

Nine of the of the 12 selenium sites of the Rab3A/rabphilin-3A complex and the two Zn^{2+} sites were found using an automated Patterson heavy-atom search method at the low-energy remote (λ_1) and peak (λ_3) wavelengths (R. W. Grosse-Kunstleve and A. T. B., unpublished data). The Zn^{2+} sites could be unambiguously assigned, since they were the only sites with a significant anomalous signal at wavelength λ_1. MAD phasing used the Phillips-Hodgson (Phillips and Hodgson, 1980) method with λ_1 as the reference wavelength at 50–226 Å resolution. Heavy-atom parameter refinement was carried out against a maximum-likelihood target function (Burling et al., 1996). The selenium and Zn^{2+} sites were simultaneously refined against the MAD data. The atomic f′ and f′′ form factor components were individually refined in order to account for the different scattering of the Zn^{2+} and selenium sites. Three SeMet sites in the rabphilin-3A effector domain were disordered: one at the N terminus, one at the C-terminal end, and one in loop L5. In the final stages of model refinement, model phases were used as a prior phase probability distribution for the heavy-atom parameter refinement. This resulted in a slightly improved experimental electron density map.

Model Building and Refinement

The initial model was built using the program O (Jones et al., 1991). The initial electron density map was obtained by MAD phasing and subsequent density modification using solvent flattening (Wang, 1985) and histogram matching (Zhang and Main, 1990) as implemented in the Crystallography and NMR System (CNS) (Brunger et al., 1998). A representative region of this electron density map is shown in Figure 6b. The high quality of the initial electron density map and known anomalous sites allowed unambiguous tracing for most of the protein backbone, side chain, and cofactor atoms. Progress was monitored with the free R value using a 10% randomly selected test set. Initial refinement consisted of several iterations of torsion angle dynamics simulated annealing (Rice and Brunger, 1994) using the MLHL target function with the experimental phases as a prior phase distribution (Pannu et al., 1998), followed by model rebuilding in O. Later, refinement consisted of iterative rounds of model building and selecting chemically reasonable water molecules in phase-combined σ_A-weighted $2F_o-F_c$ maps, conjugate gradient minimization, and individual restrained atomic B factor refinement (Hendrickson, 1985). Occupancies of disordered side chain atoms were set to zero. Refinement was carried out against the low-energy remote wavelength (λ_1). Refinement used a flat bulk solvent correction (electron density level $\rho_{sol} = 0.323$ e/Å^3, $B_{sol} = 49.7$ Å^2; Jiang and Brunger, 1994) and overall anisotropic B factor correction ($B_{11} = 6.16$ Å^2, $B_{22} = 1.16$ Å^2, $B_{33} = -7.32$ Å^2, $B_{12} = 0.0$ Å^2, $B_{13} = -1.62$ Å^2, $B_{33} = 0.0$ Å^2) at 50–2.6 Å resolution. Final model statistics are shown in Table 1.

In the crystal structure of the Rab3A/rabphilin-3A complex, the Rab3A fragment was well ordered between residues Phe-19 and Leu-191. The remaining 26 C-terminal residues were disordered in agreement with solution nuclear magnetic resonance studies carried out on Rab7 (Neu et al., 1997). The rabphilin-3A fragment was well defined for residues 44–154. Only weak electron density was found for residues 155–166. The distal regions of two rabphilin-3A loops, L2 and L5, had weak electron density, and their atomic thermal factors refined to large (∼90 Å^2) values. The final model contained 46 water molecules, one Mg^{2+}, and one GTP.

All phasing and refinement calculations were carried out using the Crystallography and NMR System (CNS) (Brunger et al., 1998).

Acknowledgments

We thank Reinhard Jahn for initiating this project; David Lambright for providing us with the coordinates of Rab3A prior to publication; Bryan Sutton for expert advice; Dirk Fasshauer, Paul Sigler, Vladimir Slepnev, Stephen Sprang, Bernd Stahl, Chris Stroupe, and Richard Yu for stimulating discussions; Craig Ogata, Mike Reese, Luke Rice, and Mark Willis for help with data collection at beamline X4a of NSLS; Paul Adams and Ralf Grosse-Kunstleve for help with CNS; and Lothar Esser for assistance in figure preparation. Beamline X4a at NSLS, a Department of Energy facility, is supported by the Howard Hughes Medical Institute. C. O. acknowledges support by an Otto Hahn fellowship of the Max-Planck-Institute for Biophysics (Frankfurt, FRG) and the Max-Planck-Society.

Received November 11, 1998; revised December 15, 1998.

References

Berlot, C.H., and Bourne, H.R. (1992). Identification of effector-activating residues of $G_{s\alpha}$. Cell *68*, 911–922.

Boguski, M.S., and McCormick, F. (1993). Proteins regulating Ras and its relatives. Nature *366*, 643–654.

Bourne, H.R., Sanders, D.A., and McCormick, F. (1991). The GTPase superfamily: conserved structure and molecular mechanism. Nature *349*, 117–127.

Brennwald, P., and Novick, P. (1993). Interactions of three domains

distinguishing the Ras-related GTP-binding proteins Ypt1 and Sec4. Nature *362*, 560–563.

Brtva, T.R., Drugan, J.K., Ghosh, S., Terrell, R.S., Campbell-Burk, S., Bell, R.M., and Der, C.J. (1995). Two distinct Raf domains mediate interactions with Ras. J. Biol. Chem. *270*, 9809–9812.

Brunger, A.T., Milburn, M.V., Tong, L., de Vos, A.M., Jancarick, K., Yamaizumi, Z., Nishimura, S., Ohtsuka, E., and Kim, S.H. (1990). Crystal structure of an active form of ras protein, a complex of a GTP analog and the h-ras p21 catalytic domain. Proc. Natl. Acad. Sci. USA *87*, 4849–4853.

Brunger, A.T., Adams, P.D., Clore, G.M., DeLano, W.L., Gros, P., Grosse-Kunstleve, R.W., Jiang, J.S., Kuszewski, J., Nilges, M., Pannu, N.S., et al. (1998). Crystallography & NMR system (CNS): a new software system for macromolecular structure determination. Acta Crystallogr. *D54*, 905–921.

Burley, S.K., and Petsko, G.A. (1985). Aromatic-aromatic interaction: a mechanism of protein structure stabilization. Science *229*, 23–28.

Burling, F.T., Weis, W.I., Flaherty, K.M., and Brunger, A.T. (1996). Direct observation of protein solvation and discrete disorder with experimental crystallographic phases. Science *271*, 72–77.

Castillo, P.E., Janz, R., Südhof, T.C., Tzounopoulos, T., Malanka, R.C., and Nicoll, R.A. (1997). Rab3A is essential for mossy fiber long-term potentiation in the hippocampus. Nature *388*, 590–593.

Chavrier, P., Gorvel, J.P., Stelzer, E., Simons, K., Gruenberg, J., and Zerial, M., (1991). Hypervariable C-terminal domain of Rab proteins acts as a targeting signal. Nature *353*, 769–772.

Chung, S.H., Song, W.J., Kim, K., Bednarski, J.J., Prestwich, G.D., and Holz, R.W. (1998). The C2 domains of rabphilin-3A specifically bind phosphatidylinositol 4,5-biphosphate containing vesicles in a Ca^{2+}-dependent manner. *In vitro* characteristics and possible significance. J. Biol. Chem. *273*, 10240–10248.

Conner, S., and Wessel, G.M. (1998). Rab3 mediates cortical granule exocytosis in the sea urchin egg. Dev. Biol. *203*, 334–344.

Der, C.J., Finkel, T., and Cooper, G.M. (1986). Biological and biochemical properties of human rasH genes mutated at codon 61. Cell *44*, 167–176.

Dumas, J.J., Zhongyuan, Z., Connolly, J.L., and Lambright, D.G. (1998). The 2.0 Å crystal structure of Rab GTPase. Structure, in press.

Esnouf, R.M. (1997). BOBSCRIPT: an extensively modified version of MOLSCRIPT that includes greatly enhanced coloring capabilities. J. Mol. Graph. Model *15*, 132–134.

Farnsworth, C.C., Kawata, M., Yoshida, Y., Takai, Y., Gelb, M.H., and Glomset, J.A. (1991). C terminus of the small GTP-binding protein smg p25A contains two geranylgeranylated cysteine residues and a methyl ester. Proc. Natl. Acad. Sci. USA *88*, 6196–6200.

Ferro-Novick, S., and Novick, P. (1993). The role of GTP-binding proteins in transport along the exocytic pathway. Annu. Rev. Cell. Biol. *9*, 575–599.

Fischer von Mollard, G., Mignery, G.A., Baumert, M., Perin, M.S., Hanson, T.J., Burger, P.M., Jahn, R., and Südhof. (1990). Rab3A is a small GTP-binding protein exclusively localized to synaptic vesicles. Proc. Natl. Acad. Sci. USA *87*, 1988–1992.

Fischer von Mollard, G., Stahl, B., Li, C., Südhof, T.C., and Jahn, R. (1994). Rab proteins in regulated exocytosis. Trend Biochem. Sci. *19*, 164–168.

Fyske, E.M., Li, C., and Südhof, T.C. (1995). Phosphorylation of rabphilin-3A by Ca^{2+}/calmodulin- and cAMP-dependent protein kinases *in vitro*. J. Neurosci. *15*, 2385–2395.

Garnier, J., Gibrat, J.F., and Robson, B. (1996). GOR secondary structure prediction method version IV. Methods Enzymol. *266*, 540–553.

Gaullier, J.-M., Simonsen, A., D'Arrigo, A., Bremnes, B., and Stenmark, H. (1998). FYVE fingers bind PtdIns(3)P. Nature *394*, 432–433.

Geppert, M., and Südhof, T.C. (1998). Rab3 and synaptotagmin: the yin and yang of synaptic membrane fusion. Annu. Rev. Neurosci. *21*, 75–95.

Geppert, M., Goda, Y., Stevens, C.F., and Südhof, T.C. (1997). The small GTP-binding protein Rab3A regulates a late step in synaptic fusion. Nature *387*, 810–814.

Gill, G.N. (1995). The enigma of LIM domains. Structure *3*, 1285–1289.

Goldberg, J. (1998). Structural basis for activiation of ARF GTPase: mechanisms of guanine nucleotide exchange and GTP-myristoyl switching. Cell *95*, 237–248.

Guan, K.L., and Dixon, J.E. (1991). Eukaryotic proteins expressed in *Escherichia coli*: an improved thrombin cleavage and purification procedure of fusion proteins with glutathione S-transferase. Anal. Biochem. *192*, 262–267.

Hendrickson, W.A. (1985). Stereochemically restrained refinement of macromolecular structures. Methods Enzymol. *115*, 252–270.

Hendrickson, W.A. (1991). Determination of macromolecular structures from anomalous diffraction of synchrotron radiation. Science *254*, 51–58.

Holm, L., and Sander, C. (1993). Protein structure comparison by alignment of distance matrices. J. Mol. Biol. *233*, 123–138.

Huang, L., Hofer, F., Martin, G.S., and Kim, S.H. (1998). Structural basis for the interaction of Ras with RalGDS. Nat. Struct. Biol. *5*, 422–426.

Jiang, J.-S., and Brunger, A.T. (1994). Protein hydration observed by x-ray diffraction: solvation properties of penicillopepsin and neuramidase crystal structures. J. Mol. Biol. *243*, 100–115.

Johnson, J.D., Zhang, W., Rudnick, A., Rutter, W.J., and German, M.S. (1997). Transcriptional synergy between LIM-homeodomain proteins and basic helix-loop-helix proteins: the LIM2 domain determines specificity. Mol. Cell. Biol. *17*, 3488–3496.

Jones, T.A., Zou, J.Y., Cowan, S., and Kjeldgaard, M. (1991). Improved methods for building protein models in electron density maps and the location of errors in these models. Acta Crystallogr. *A47*, 110–119.

Kato, M., Sasaki, T., Imazumi, K., Takahashi, J., Araki, H., Shiritaki, Y., Matsuura, A., Ishida, A., Fujisawa, H., and Takai, Y. (1994). Phosphorylation of rabphilin-3A by calmodulin-dependent protein kinase II. Biochem. Biophys. Res. Commun. *205*, 1776–1784.

Kato, M., Sasaki, T., Nakanishi, H., Nishioka, H., Imamura, M., and Takai, Y. (1996). Physical and functional interaction of rabphilin-3A with α-actinin. J. Biol. Chem. *271*, 31775–31778.

Kotake, K., Ozaki, N., Mizuta, M., Sekiya, S., Inaga, N., and Seino, S. (1997). Noc2, a putative zinc finger protein involved in exocytosis in endocrine cells. J. Biol. Chem. *272*, 29407–29419.

Kraulis, P. (1996). MOLSCRIPT: a program to produce both detailed and schematic plots of macromolecular structures. J. Appl. Crystallogr. *24*, 946–950.

Leahy, D.J., Erickson, H.P., Aukhil, I., Joshi, P., and Hendrickson, W.A. (1994). Crystallization of a fragment of human fibronectin: introduction of methionine by site-directed mutagenesis to allow phasing via seleniomethionine. Proteins: Struct. Funct. Genet. *19*, 48–54.

Li, C., Takei, K., Geppert, M., Daniell, L., Stenius, K., Chapman, E.R., Jahn, R., De Camilli, P., and Südhof, T.C. (1994). Synaptic targeting of rabphilin-3a, a synaptic vesicle Ca^{2+}/phospholipid-binding protein, depends on Rab3A/3C. Neuron *13*, 885–898.

Marshall, M.S. (1993). The effector interaction of p21ras. Trends Biochem. Sci. *18*, 250–254.

Mayer, A., and Wickner, W. (1997). Docking of yeast vacuoles is catalyzed by the ras-like GTPase Ypt7p after symmetric priming by sec18p (NSF). J. Cell. Biol. *136*, 307–317.

McKiernan, C.J., Stabila, P.F., and Macara, I.G. (1996). Role of the Rab3A-binding domain in targeting of rabphilin-3a to vesicle membranes of PC12 cells. Mol. Cell. Biol. *16*, 4985–4995.

Milburn, M.V., Tong, L., deVos, A.M., Brunger, A.T., Yamaizumi, Z., Nishimura, S., and Kim, S.-H (1990). Molecular switch for signal transduction: structural differences between active and inactive forms of protooncogenic ras proteins. Science *247*, 939–945.

Mott, H.R., Carpenter, J.W., Zhong, S., Ghosh, S., and Bell, R.M. (1996). The solution structure of the Raf-1 cysteine-rich domain: a novel ras and phospholipid binding site. Proc. Natl. Acad. Sci. USA *93*, 8312–8317.

Nasser, N., Horn, G., Herrmann, C., Scherer, A., McCormick, F., and Wittinghofer, A. (1995). The 2.2 Å crystal structure of the Ras-binding

domain of the serine/threonine kinase c-Raf1 in complex with Rap1A and a GTP analogue. Nature *375*, 554–560.

Neu, M., Brachvogel, V., Oschkinat, H., Zerial, M., and Metcalf, P. (1997). Rab7: NMR and kinetic analysis of intact and C-terminal truncated constructs. Proteins: Struct. Funct. Genet. *27*, 204–209.

Nicholls, A., Sharp, K.A., and Honig, B. (1991). Protein folding and association: insights from the interfacial and thermodynamic properties of hydrocarbons. Proteins: Struct. Funct. Genet. *11*, 281–296.

Novick, P., and Zerial, M. (1997). The diversity of Rab proteins in vesicle transport. Curr. Opin. Cell. Biol. *9*, 496–504.

Nuoffer, C., and Balch, W.E. (1994). GTPases: multifunctional molecular switches regulating vesicular traffic. Annu. Rev. Biochem. *63*, 949–990.

Otwinowski, Z., and Minor, W. (1998). Processing of X-ray diffraction data collected in oscillation mode. Methods Enzymol. *276*, 307–326.

Pai, E.F., Krengel, U., Pesko, G.A., Goody, R.S., Kabsch, W., and Wittinghofer, A. (1990). A refined crystal structure of the triphosphate conformation of h-ras p21 at 1.35 Å resolution: implications for the mechanism of GTP hydrolysis. EMBO J. *9*, 2351–2359.

Pannu, N.S., Murshudov, G.N., Dodson, E.J., and Read, R.J. (1998). Incorporation of prior phase information strengthens maximum likelihood structural refinement. Acta Crystallogr. D. *54*, 1285–1294.

Patki, V., Lawe, D.C., Corvera, S., Virbasius, J.V., and Chawla, A. (1998). A functional PtdIns(3)P-binding motif. Nature *394*, 433–434.

Pérez-Alvarado, G.C., Kosa, J.L., Louis, H.A., Beckerle, M.C., Winge, D.R., and Summers, M.F. (1996). Structure of the cysteine-rich intestinal protein, CRIP. J. Mol. Biol. *257*, 153–174.

Pfeffer, S.R. (1994). Rab GTPases: master regulators of membrane trafficking. Curr. Opin. Cell. Biol. *6*, 522–526.

Pfeffer, S.R. (1996). Transport vesicle docking: SNARE and associates. Annu. Rev. Cell Biol. Dev. Biol. *12*, 441–461.

Phillips, J.C., and Hodgson, K.O. (1980). The use of anomalous scattering effects to phase diffraction patterns from macromolecules. Acta Crystallogr. *A36*, 856–864.

Polakis, P., and McCormick, F. (1993). Structural requirement for the interaction of p21ras with GAP, exchange factors, and its biological effector target. J. Biol. Chem. *268*, 9157–9160.

Prive, G.G., Milburn, M.V., Tong, L., de Vos, A.M., Yamaizumi, Z, Nishimura, S., and Kim, S.H. (1992). X-ray crystal structures of transforming p21 ras mutants suggest a transition-state stabilization mechanism for GTP hydrolysis. Proc. Natl. Acad. Sci. USA *89*, 3649–3653.

Rarick, H.M., Artemyev, N.O., and Hamm, H.E. (1992). A site on rod G protein α subunit that mediates effector activation. Science *256*, 1031–1033.

Rice, L.M., and Brunger, A.T. (1994). Torsion angle dynamics: reduced variable conformational sampling enhances crystallographic structure refinement. Proteins: Struct. Funct. Genet. *19*, 277–290.

Sasaki, T., Kikuchi, A., Araki, S., Hata, Y., Isomura, M., Kuroda, S., and Takai, Y. (1990). Purification and characterization from bovine brain cytosol of a protein that inhibits the dissociation of GDP from and the subsequent binding of GTP to smg p25A, a ras p21-like GTP-binding protein. J. Biol. Chem. *265*, 2332–2337.

Schmeichel, K.L., and Beckerle, M.C. (1994). The LIM is a modular protein-binding interface. Cell *79*, 211–219.

Schmeichel, K.L., and Beckerle, M.C. (1998). LIM domains of cysteine-rich protein 1 (CRP1) are essential for its zyxin-binding function. Biochem. J. *331*, 885–892.

Shirataki, H., Kaibuchi, K., Sakoda, T., Kishida, S., Yamaguchi, T., Wada, K., Miyazaki, M., and Takai, Y. (1993). Rabphilin-3A, a putative target protein for smg p25A/Rab3A p25 small GTP-binding protein related to synaptotagmin. Mol. Cell. Biol. *13*, 2061–2068.

Sigler, P.B. (1996). Stereochemistry of activation and GTPase mechanism of $G_{t\alpha}$ at 1.8 Å resolution. In Structure and Function of 7TM receptors, T.W. Schwarz, S.A. Hjorth, and J. Sandholm, eds. (Copenhagen: Munksgaard). Alfred Benzon Symposium *39*, pp. 17–29.

Simons, K., and Zerial, M. (1993). Rab proteins and the road maps for intracellular transport. Neuron *11*, 789–799.

Simonsen, A., Lippé, R., Christoforidis, S., Gaullier, J.-M., Brech, A., Callaghan, J., Toh, B.-H., Murphy, C., Zerial, M., and Stenmark, H. (1998). EEA1 links PI(3)K function to Rab5 regulation of endosome fusion. Nature *394*, 494–498.

Søgaard, M., Tani, K., Ye, R.R., Geromanos, S., Tempst, P., Kirchhausen, T., Rothman, J.E., and Söllner, T. (1994). A Rab protein is required for the assembly of SNARE complexes in the docking of transport vesicles. Cell *78*, 937–948.

Sprang, S.R. (1997a). G protein mechanisms: insights from structural analysis. Annu. Rev. Biochem. *66*, 639–678.

Sprang, S.R. (1997b). G proteins, effectors and GAPs: structure and mechanism. Curr. Opin. Struct. Biol. *7*, 849–856.

Stahl, B., Chou, J.H., Li, C., Südhof, T.C., and Jahn, R. (1996). Rab3 reversibly recruits rabphilin to synaptic vesicles by a mechanism analogous to raf recruitment by ras. EMBO J. *15*, 1799–1809.

Stenmark, H., Valencia, A., Martinez, O., Ulrich, O., Goud, B., and Zerial, M. (1994). Distinct structural elements of rab5 define its functional specificity. EMBO J. *13*, 575–583.

Sunahara, R.K., Tesmer, J.J.G., Gilman, A.G., and Sprang, S.R. (1997). Crystal structure of the adenylyl cyclase activator $G_{s\alpha}$. Science *278*, 1943–1947.

Sutton, R.B., Davletov, B.A., Berhuis, A.M., Südhof, T.C., and Sprang, S.R. (1995). Structure of the first C2 domain of synaptotagmin I: a novel Ca^{2+}/phospholipid-binding fold. Cell *80*, 929–938.

Tesmer, J.J., Sunahara, R.K., Gilman, A.G., and Sprang, S.R. (1997). Crystal structure of the catalytic domains of adenylyl cyclase in complex with $G_{s\alpha}$-GTPγS. Science *278*, 1907–1916.

The POV-ray team. (1998). Pov-ray—the persistence of vision raytracer. http://www.povray.org/.

Tong, L., Milburn, M.V., De Vos, A.M., and Kim, S.-H. (1989). Structure of *ras* protein. Science *245*, 244.

Ungermann, C., Sato, K., and Wickner, W. (1998). Defining the function of *trans*-SNARE pairs. Nature *396*, 543–548.

Wang, B.C. (1985). Resolution of phase ambiguity in macromolecular crystallography. Methods Enzymol. *115*, 90–112.

Wang, Y., Okamoto, M., Schmitz, F., Hofmann, K., and Südhof, T.C. (1997). Rim is a putative Rab3 effector in regulating synaptic-vesicle fusion. Nature *388*, 593–598.

Wiedemann, C., and Cockcroft, S. (1998). Sticky fingers grab a lipid. Nature *394*, 426–427.

Yamaguchi, T., Shirataki, H., Kishida, S., Miyazaki, M., Nishikawa, J., Wada, K., Numata, S., Kaibuchi, K., and Takai, Y. (1993). Two functionally different domains of rabphilin-3a, Rab3A, p25/smg p25A-binding and phospholipid- and Ca^{2+}-binding domains. J. Biol. Chem. *268*, 27164–27170.

Zhang, K.Y.J., and Main, P. (1990). Histogram matching as a new density modification technique for phase refinement and extension of protein molecules. Acta Crystallogr. A *46*, 41–46.

Brookhaven Protein Data Bank ID Code

The coordinates and structure factors have been deposited with the ID code 1zbd and are immediately available on the web page http://atb.csb.yale.edu.